Flexible Octopus-Shaped Hydrogel Particles for Specific Cell Capture

*Lynna Chen, Harry Z. An, Ramin Haghgooie, Aaron T. Shank, Joseph M. Martel, Mehmet Toner, and Patrick S. Doyle**

The physical properties of micro- and nanoparticles—size, shape, and stiffness—play an important role in determining their function in applications such as medical diagnostics and drug delivery.[1–3] Changing a synthetic particle's shape and elasticity can influence the way the particle moves through the body and alters its interactions with individual cells.

Recent advances in fabrication techniques for nonspherical, soft particles, including microfluidic techniques,[4,5] nonwetting template molding (PRINT),[6] electrohydrodynamic jetting,[7] and film stretching,[8] have enabled systematic studies of how physical properties of microparticles affect circulation in the body,[3,9] cellular internalization,[10] and passage through epithelial layers.[11] These studies have outlined important new design criteria for effective drug delivery vehicles. For example, flexible particles are more effective at squeezing through small capillaries in the bloodstream, increasing their overall circulation time and enhancing biodistribution compared to their rigid counterparts.[9,12] Other studies have shown that a particle's shape affects its interactions with individual cells,[10,13] for example, antibody displaying rod-shaped particles shows increased specific uptake by cancer cells compared to spherical particles.[14] In a similar vein, recent work has demonstrated the importance of rationally designing the shape of pillars used in deterministic lateral displacement microfluidic devices to improve the label-free separation of nonspherical biological entities (e.g., red blood cells and bacteria).[15,16] Unconventional I-shaped pillars were shown to improve the separation efficiency of disk and rod-shaped cells by inducing rotational movements.[15,16] These studies highlight the importance of designing material shape and elasticity for interfacing with biological cells.

Despite significant advances in this field with regard to designing particle shape for drug delivery and pillar shape for cell separation, the role of both shape and elasticity on particle function in many other biological environments remains to be studied. Recent reviews have highlighted the importance of designing the physical and chemical properties of material interfaces for cell capture, the first step in many diagnostic applications.[17,18] However, to date, there have been no controlled studies that examine the advantages of custom-shape, flexible particles for affinity-based capture of specific cell populations.

A strong motivation for designing new cell-capture strategies is the detection and characterization of circulating tumor cells (CTCs), the cells that are shed from tumors and move through the bloodstream, contributing to cancer metastasis.[19,20] Ideally, it would be possible to isolate viable CTCs from a patient's blood sample, characterize the cells with molecular diagnostics, and subsequently culture the cells for analysis of drug sensitivity. This would enable less invasive alternatives to biopsies for cancer diagnosis and optimization of treatment regimens. Unfortunately, achieving this goal remains a challenge because CTCs are extremely rare (0.3–100 CTCs mL^{-1} of whole blood in cancer patients, amongst millions of white blood cells and billions of red blood cells), heterogeneous in nature, and difficult to keep viable for analysis after isolation.[17,21–23] Techniques that currently exist for CTC detection and separation include cell-affinity chromatography (i.e., capture using antibodies immobilized in microfluidic channels),[24–26] immunomagnetic sorting (i.e., capture by antibody-coated magnetic particles suspended in solution),[27] size-based sorting (i.e., separation based on the larger size of CTCs compared to blood cells),[28] and dielectrophoretic techniques (i.e., separation based on differing cell responses to electric fields).[27,29,30] Microfluidic negative depletion of blood cells to isolate CTCs has also been reported.[31,32]

Recently, microfluidic approaches for CTC capture have been gaining popularity because of large surface area-to-volume ratios and multiplexing capabilities.[30,33] However, particle-based approaches can offer more flexibility for transport and manipulation of cells, eliminate the need for

L. Chen
Department of Biological Engineering
Massachusetts Institute of Technology
77 Massachusetts Avenue, Cambridge, MA 02139, USA
Dr. H. Z. An, Prof. P. S. Doyle
Department of Chemical Engineering
Massachusetts Institute of Technology
77 Massachusetts Avenue, Cambridge, MA 02139, USA
E-mail: pdoyle@mit.edu
Dr. R. Haghgooie
General Fluidics
34 Anderson St., Ste 5, Boston, MA 02114, USA
A. T. Shank, Dr. J. M. Martel, Prof. M. Toner
Center for Engineering in Medicine
Massachusetts General Hospital
Harvard Medical School
Building 114, 16th Street, Charlestown, MA 02129, USA

DOI: 10.1002/smll.201600163

www.MaterialsViews.com

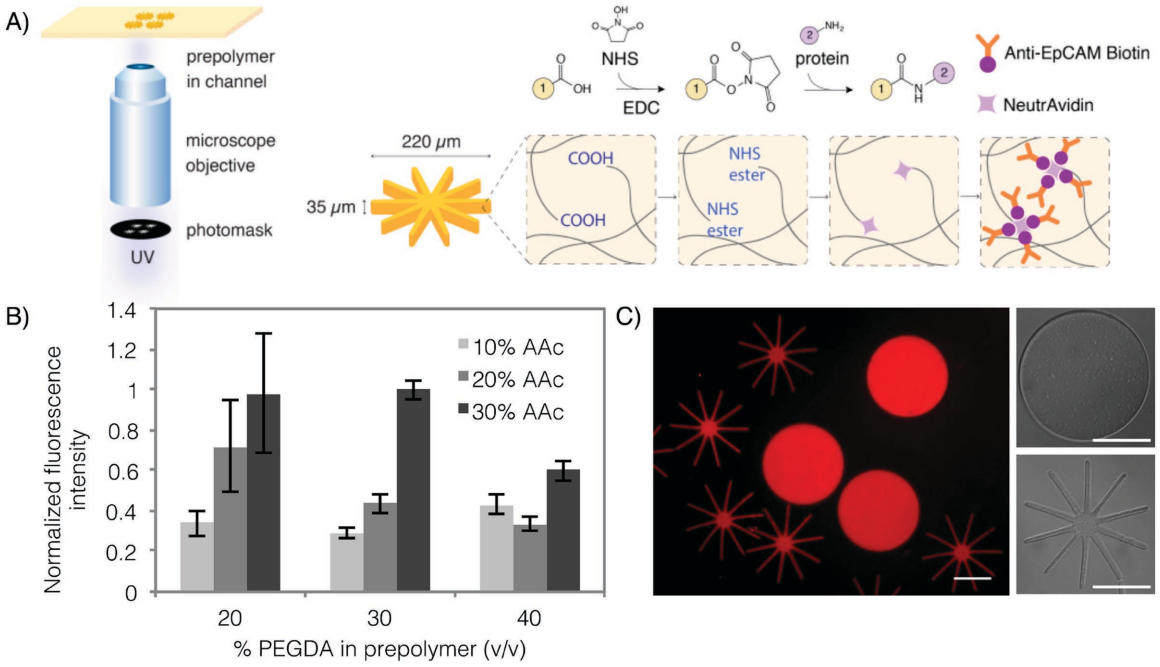

Figure 1. Fabrication of antibody-functionalized hydrogel microparticles. A) PEGDA is copolymerized with AAc to fabricate particles with photomask-defined shapes via SFL. Carboxylic acid groups of PEGDA-AAc particles are functionalized with NeutrAvidin using carbodiimide (EDC) chemistry, which can then be conjugated with biotinylated anti-EpCAM. In the schematic, side group 1 corresponds to the rest of the PEGDA particle, while side group 2 is NeutrAvidin. B) The optimal prepolymer composition (30% PEGDA, 30% AAc) was chosen to achieve maximum antibody functionalization with good particle uniformity. Functionalization capacity was determined by measuring the intensity of a biotinylated fluorophore used to label the functionalized particles. C) Fluorescent and bright-field images of disk and octopus-shaped particles fabricated using this method. The fluorescence of these particles is due to the addition of rhodamine acrylate in the prepolymer. Scale bars are 100 μm.

functionalization of individual channels, and be used synergistically with microfluidic systems.[34–36] Customizable hydrogel microparticles have additional advantages: they are biocompatible, easy to functionalize—with antibodies, aptamers,[37] DNA,[38] magnetic nanoparticles,[39] or drug-loaded nanoemulsions[40]—and can be fabricated with tailored shape and size to maximize available capture area.

In this work, we explore how to leverage particle shape to improve capture efficiency of cells expressing epithelial cell adhesion molecule (EpCAM), a protein that is frequently expressed by CTCs.[41] We fabricate hydrogel microparticles with mask-defined shapes via stop flow lithography (SFL),[4,42] and demonstrate specific capture of EpCAM-expressing cancer cells in solution using functionalized particles. By systematically varying particle shape, we demonstrate how surface area, hydrodynamic effects, and steric constraints affect cell capture efficiency. Drawing upon previous work describing the influence of particle shape on mechanical flexibility,[43] we proceed to investigate how cell-laden particles of different shapes traverse through microfluidic constrictions, and show the effect of shape-induced flexibility on the retention of captured cells. The microfluidic constrictions act as in vitro models to allow study of particle passage in simulated biological environments.[44]

This study is a demonstration of how microparticle shape can be exploited to increase cell-capture efficiency and improve cell retention in flow through microfluidic constrictions. Our results indicate that the physical parameters of shape and flexibility should be considered when designing microparticles for cell-capture-based diagnostic applications.

The particle synthesis and functionalization procedure is illustrated in **Figure 1**A. We fabricate poly(ethylene) glycol (PEG)-based hydrogel particles via SFL. In SFL, a prepolymer flowing through a microfluidic channel is polymerized by UV light in a mask-defined shape.[4,42] Using this technique, it is possible to make custom-shape microparticles with uniform shape and size, in a high-throughput manner. We fabricate particles using poly(ethylene glycol) diacrylate (PEGDA, M_n = 700 g mol^{-1}), copolymerized with acrylic acid (AAc). Our prepolymer solution also consists of a photoinitiator, and PEG (MW = 200 g mol^{-1}), which acts as a porogen to increase hydrogel porosity and improve mechanical flexibility.[45]

The carboxylic acid groups from the copolymerized AAc allow the hydrogel to be easily functionalized with proteins using carbodiimide chemistry.[46] The carboxylic acid groups are activated to NHS (*N*-hydroxysuccinimide) ester groups, which can then couple with primary amines present in the lysine residues of any protein. We covalently conjugated NeutrAvidin, a neutral form of avidin with less nonspecific binding, to our hydrogel particles. The particles were then functionalized with a biotinylated antibody against EpCAM (anti-EpCAM biotin). Surface-bound anti-EpCAM biotin enables interactions between cells and particles. This two-step functionalization strategy enables particle functionalization by any biotinylated probe, improves protein uniformity throughout the hydrogel, and ensures no changes to antibody

small 2016,
DOI: 10.1002/smll.201600163

function due to direct covalent conjugation. Antibodies conjugated to hydrogel particles in this manner retain their activity after more than two months of storage (Figure S1, Supporting Information).

To ensure optimal particle functionalization, we tested the effect of different particle prepolymer compositions on the resulting degree of NeutrAvidin conjugation. In Figure 1B, we varied the volume percent of PEGDA and AAc present in the prepolymer solution and tested the level of functionalization by labeling with excess biotinylated fluorophore. The fluorescence intensity observed should correlate to the amount of anti-EpCAM biotin bound to the particles. As expected, increasing the amount of AAc in the prepolymer increased the level of functionalization by increasing the number of carboxylic acid groups available for conjugation. For particles fabricated using more than 20% (v/v) AAc in the prepolymer, increasing the amount of PEGDA decreased the level of functionalization. This may be due to the tighter mesh of the hydrogel, which sterically hinders the conjugation of NeutrAvidin, or the diffusion of the fluorescent probe into the gel. Based on our results, we chose an optimized prepolymer composition of 30% PEGDA and 30% AAc to achieve highly functionalized particles with good reproducibility.

In Figure 1C, we show particles synthesized using our chosen prepolymer composition, demonstrating excellent uniformity in particle size and shape. We were able to fabricate multiarm particles with finely patterned in-plane features (arm length to width ratio of 8:1), with the same nominal outer diameter as more conventional disk-shaped particles (diameter = 220 µm). Our multiarm particle geometry was inspired by shapes found in nature—both in animals and plants, as well as microscale organisms and tissues. For example, octopus and squid use suction cup-covered arms for capturing prey and some plants (e.g., sundews) use sticky tentacles to catch insects. In our own bodies, finger-like protrusions on cell membranes of some epithelial cells called microvilli are useful for absorbing nutrients and improving cellular adhesion.[47] In all of these examples, the flexible, mobile nature of the arms or protrusions is critical for their function. Inspired by these biological motifs, we designed our "octopus particles" with thin arms arranged radially around a central core. It is worth noting that our synthetic multiarm particle geometry resembles much smaller star polymers, a common polymer architecture consisting of many linear polymer chains ("arms") connected to a central core. Star polymers demonstrate improved response to stimuli due to high functionalization density.[48] We predicted that the high aspect ratio arms on our particles would be well suited for cell capture due to their high surface area and mechanical flexibility.

In order to test whether our functionalized octopus particles could capture cells of interest, we performed experiments using two cell lines: SKBR3s—breast cancer cells with high expression of EpCAM (EpCAM+, dyed blue for all experiments) and SKMEL28s—melanoma cells that do not express the protein (EpCAM–, dyed green for all experiments).[49,50] **Figure 2**A shows that functionalized particles effectively capture EpCAM+ cells, while demonstrating no nonspecific adherence to EpCAM– cells. As another negative control, we incubated plain PEGDA-AAc particles (before functionalization) with the cells under identical conditions and found no capture of either cell type. This confirms the bio-inert nature of PEGDA particles,[51] and shows that the copolymerized AAc does not lead to any nonspecific interactions. Other groups have also shown PEG-based and PEG-functionalized hydrogels to be suitable materials for antibody-based cell capture, and have demonstrated triggered cell release by breaking photolabile or physical crosslinks

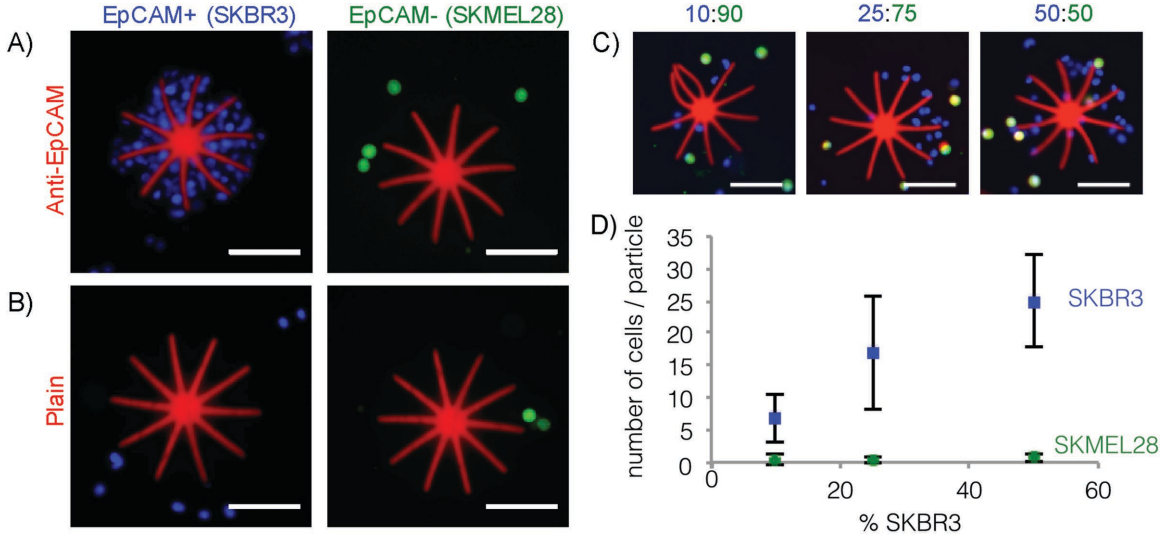

Figure 2. Cell capture by octopus particles. A) EpCAM-expressing cells (SKBR3s, blue) are captured by anti-EpCAM functionalized particles, while non-EpCAM expressing cells (SKMEL28s, green) do not adhere. B) Plain, nonfunctionalized particles (PEGDA-AAc) do not capture either cell type. C) Particles successfully capture SKBR3s in mixed cell solutions (ratio of SKBR3 to SKMEL28 are indicated above images, total cell concentration = 100 000 cells mL^{-1}). D) Quantification of the number of SKBR3s and SKMEL28s captured per particle in the mixed cell solutions corresponding to the representative images in part C (averages are plotted ± standard deviation, $N = 20$). All scale bars are 100 µm. Figure S2 (Supporting Information) shows multiple particles in the same image for the 50:50 mixed cell incubation condition.

DOI: 10.1002/smll.201600163

within the gel.[52–54] Previously, photopatterned PEG structures have also been used to capture cells from flowing solutions in microfluidic devices.[55]

To determine quantitative trends between solution cell concentration and number of cells captured, we incubated the octopus particles in mixed cell solutions containing different ratios of SKBR3s to SKMEL28s. We counted the cells attached to the top and side surfaces of the particles, ignoring the hidden bottom surfaces, and distinguished between the two cells types by fluorescence color. It should be noted that images in Figure 2C show a higher number of SKBR3s compared to SKMEL28s, regardless of cell incubation concentrations, due to the imaging setup. By imaging particles in a small drop of solution immediately after they settle on a microscope slide, cells attached to the particles are in focus, while cells suspended in solution are not. In the cell concentration range between 10 000 and 50 000 SKBR3s mL^{-1} (10%–50% SKBR3s, total cell concentration: 100 000 cells mL^{-1}), we saw an almost linear correlation between the number of cells attached to our particles and the concentration of cells in solution. The data plotted in Figure 2D corresponds to an SKBR3 capture efficiency of ≈40%, 40%, and 30% for the 10:90, 25:75, and 50:50 incubation conditions, respectively. While the concentrations used in this experiment are not representative of clinical CTC concentrations expected in patient blood samples, this proof-of-concept demonstration indicates that our particles are able to selectively capture cells of interest in mixed cell populations and are quantitatively sensitive to changes in cell concentration. Optimization of incubation conditions is expected to increase the recovery rate of target cells, bringing us closer to clinically relevant cell concentrations. Increasing the particle-to-cell ratio will also help to capture rare cells; in future work, particle production can be scaled-up using the recently developed contact flow lithography technique.[56]

Motivated by our observations that octopus particles were effective at capturing SKBR3s, we proceeded to investigate the effect of particle shape on cell capture. We designed shapes such that all of them could be circumscribed by a 220 μm diameter circle, and polymerized all particles using the same prepolymer, microfluidic channel design, and UV exposure conditions. All particles were ≈35 μm tall and expected to have similar surface chemistry and degree of functionalization. First, we made particles with different number of arms: 2, 4, 6, 8, and 10. As expected, the number of cells captured on the particles increased with number of arms (**Figure 3**A), which also corresponds to increasing total surface area (Table S1, Supporting Information). However, this curve plateaus when the number of arms exceeds eight. At this point, steric hindrance prevents more cells from attaching to the particles as the gap between neighboring arms becomes comparable in dimension to the cell diameter.

We proceeded to normalize the number of cells attached to each particle by the particle total surface area (Figure 3B; surface areas shown in Table S1 in the Supporting Information; data before normalization shown in Figure S3 in the Supporting Information), and confirmed that cell capture depends on more than just surface area—other shape effects must also play a role. We tested three additional shapes,

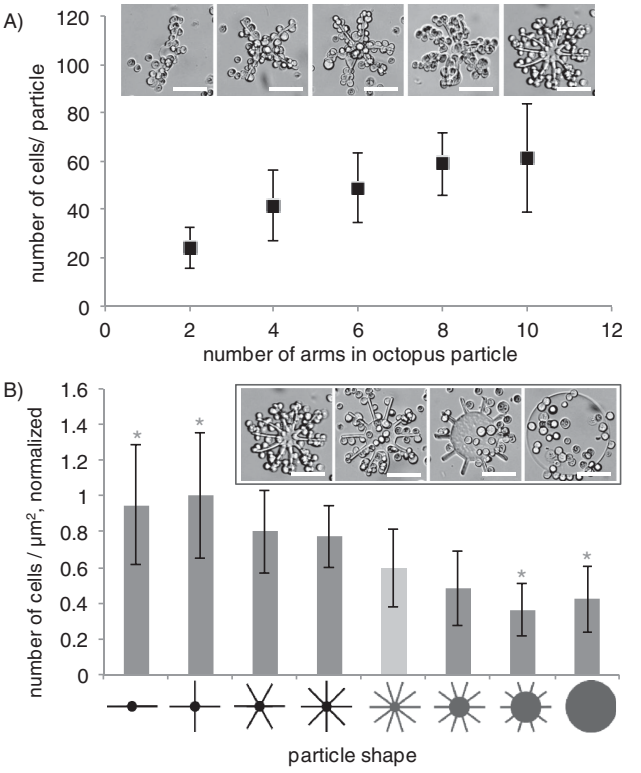

Figure 3. Cell capture by different shapes. A) Number of SKBR3s captured by octopus particles with two, four, six, eight, and ten arms. Representative bright-field images are shown for each data point. B) Number of captured SKBR3s normalized by individual particle total surface area (and normalized across all shapes) are plotted for eight different shapes with the same nominal outer diameter (including the five shapes from part (A)). Representative bright-field images are shown for the 10 arm and disk particle shapes. Averages are plotted ± standard deviation, $N = 13$. (*$P < 0.05$ by Student's t-test with Bonferroni correction, compared to the ten-arm particle indicated by the light gray bar.) Scale bars are 100 μm.

where we progressively increased the core diameter at the expense of arm length, maintaining the same outer particle diameter. In the extreme case, the arms were eliminated altogether, and we tested the cell capture ability of a solid disk. In Figure 3B, the particle shapes are arranged by increasing in-plane area (or top surface area, as shown in Table S1 in the Supporting Information). We see a general trend where cells captured per μm^2 decreases as top surface area increases. We predict that hydrodynamic effects are responsible for this trend. From a simplified point of view, we can say that the in-plane particle area alters the streamlines of the passing cell-containing fluid when particles and cells are mixed gently in solution. The disk particle displaces the most fluid as it moves in solution, making it less likely for cells to come into contact with the particle surface. This is the same underlying concept as strategies that vary microfluidic device geometry to maximize contact between flowing CTCs and antibody-coated surfaces (e.g., microposts,[25,57] herringbone structures[23]). Based on our results, it appears that octopus particles, with a small core and high aspect ratio arms that are far enough apart to allow cell-containing fluid to flow between them, are better suited to capturing cells in solution than disk particles.

small 2016,
DOI: 10.1002/smll.201600163

small NANO MICRO

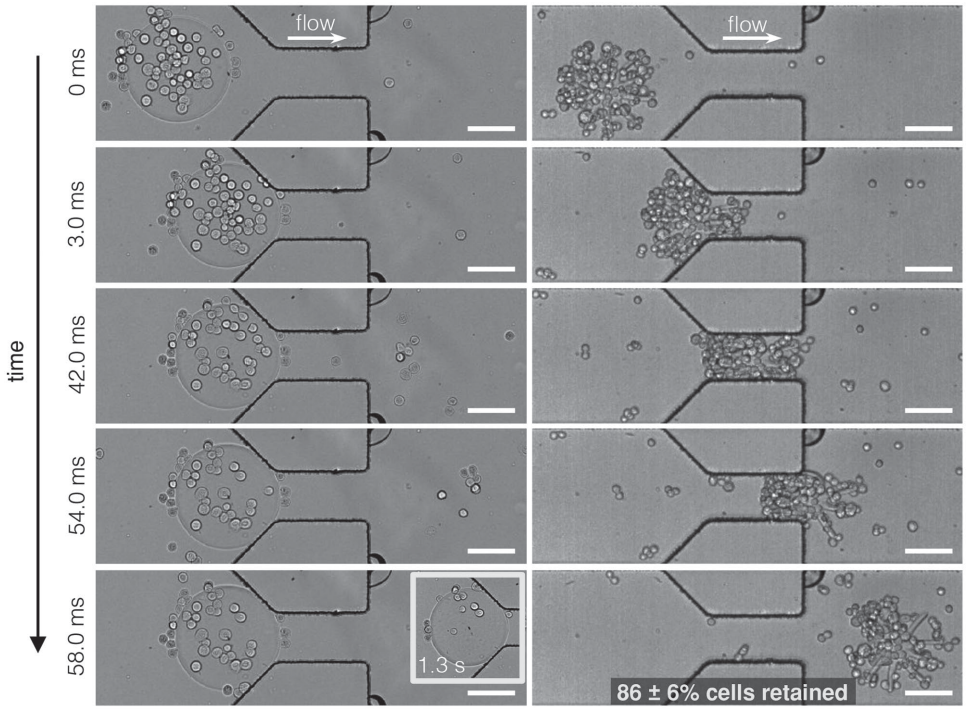

Figure 4. Particle flow through microfluidic constrictions. Still images from representative high-speed videos (Videos S1 and S2, Supporting Information) of cell-laden disk and octopus particles flowing through a microfluidic constriction (narrow part of channel is 100 μm wide). Flow was driven by a syringe pump at a rate of 20 μL min^{-1}. Disks are unable to pass through the constriction while octopus particles pass through easily. The inset shows that after 1.3 s, the disk remains stuck at the constriction entrance with few cells remaining. Octopus particles retain 86% of captured cells after passing through the constriction ($N = 8$). Scale bars are 100 μm.

After capturing cells on particles of different shape, we compared the behavior of ten-arm octopus particles and disk particles during flow through a microfluidic constriction. Microfluidic channels are often used as models for blood capillaries to test the deformability of red blood cells and synthetic particles in order to predict their behavior in the bloodstream.[44] We designed microfluidic constrictions that are just less than half the width of our particle diameter—these relative dimensions are similar to what red blood cells may experience when passing through narrow capillaries.

Figure 4 shows a series of frames from two representative high-speed videos (Videos S1 and S2, Supporting Information) of a disk and an octopus particle (both 220 μm in diameter, 35 μm tall) passing through a channel containing a narrow constriction (100 μm wide × 200 μm long × 60 μm tall). At a syringe pump-driven flow rate of 20 μL min^{-1}, the disk was unable to pass through the constriction, while the octopus passed through easily. The thin arms of the octopus are able to bend, allowing the particle to move through the narrow constriction in less than 1/10th of a second, while holding onto the majority of cells. The disk, on the other hand, was stuck at the entrance of the constriction and the continuous shear force of the fluid flowing past the particle stripped away most of the attached cells after 1 s. The disk remained stuck at the entrance of the constriction after several minutes of flow. We found that octopus particles retained an average of 86% of captured cells after passing through the constriction and that the direction of passage did not influence this behavior (Figure S4, Supporting Information).

We also studied the passage of taller disks (220 μm diameter, 55 μm tall) through the constrictions at increased flow rates of 1 mL min^{-1} (Figure S5, Supporting Information). At this flow rate, the disks compressed to pass through the constriction in ≈5 s, but the majority of cells were stripped off in the process (6% cells were retained on average).

We expect that the cells attached to the octopus particles remain viable after passage through the constriction at low to moderate flow rates. First, PEG hydrogels are biocompatible and do not affect the viability of captured cells.[53,55] Second, cell capture and release on EpCAM-functionalized hydrogels in PDMS microfluidic channels has been previously shown to have no significant effect on cell viability or proliferative potential.[24] Lastly, at a flow rate of 20 μL min^{-1}, we estimate the wall shear stress in the constriction to be on the order of 50 dyne cm^{-2}, within the range of physiological shear stress in the arterial vascular network (10–70 dyne cm^{-2}).[58] The constriction only causes deformation of the flexible particles, not of the cells.

It is evident that geometry affects a particle's overall deformability when passing through a microfluidic constriction. This is supported by a previous study showing that particle shape affects mechanical flexibility as well as mode of passage for particles traveling through a microfluidic constriction.[43] Our observations on the effect of particle shape on retention of captured cells may be useful for recovery of specific cell populations in microfluidic systems, or future in vivo applications involving particles traveling through the bloodstream.

DOI: 10.1002/smll.201600163

In conclusion, we demonstrate the use of custom-shape, flexible hydrogel microparticles for specific antibody-based cell capture. We believe this approach has many advantages, including high-throughput particle synthesis,[56] easy functionalization with various probes, potential for synergistic use with microfluidic devices for downstream analysis of captured cells, and subsequent culture of isolated cells directly on particle substrates.[59] As one example, our system may be advantageous for addressing the ongoing challenge of CTC heterogeneity, which makes efficient capture difficult and results in isolated cells that play different functional roles.[17] Using customizable microparticles that can be identified by a geometric or color-defined barcode,[38,60,61] we could functionalize several groups of particles using different CTC biomarkers (e.g., EpCAM, HER2 (human epidermal growth factor receptor 2), EGFR (epidermal growth factor receptor), MUC-1 (mucin-1)), enabling downstream characterization of CTC populations with different biochemical properties.

In this work, we show that particle shape is one important design criterion for maximizing cell-capture efficiency. Specifically, we show that octopus particles can capture more cells than similarly sized disks, by increasing cell–particle interactions through increased total surface area as well as improved hydrodynamic geometry. In addition, the effect of shape on overall particle deformability and retention of captured cells is demonstrated using a model microfluidic constriction. This work highlights the importance of shape and flexibility for particle-based cell-capture applications.

Experimental Section

Materials: Poly(ethylene glycol) diacrylate (M_n = 700 g mol^{-1}), acrylic acid (anhydrous, ≥99.0%), poly(ethylene glycol) (M_n = 200 g mol^{-1}), 2-hydroxy-2-methyl-1-phenyl-propan-1-one (Darocur 1173), *N*-(3-dimethylaminopropyl)-*N*′-ethylcarbodiimide hydrochloride (EDC, ≥ 99.0%), and *N*-hydroxysuccinimide (NHS, 98%) were purchased from Sigma-Aldrich and used as received. Methacryloxyethyl thiocarbomoyl rhodamine B ($\lambda_{ex}/\lambda_{em}$ = 548/570 nm, Polysciences) was dissolved in poly(ethylene glycol) at a concentration of 1 mg mL^{-1}. NeutrAvidin (Thermo Fisher) was diluted with PBS (phosphate buffered saline) to a concentration of 5 mg mL^{-1} and the stock solution was stored at 4 °C. Anti-Human CD326 (EpCAM) Biotin (0.5 mg mL^{-1}, Affymetrix) was used as received. PBST (PBS with surfactant Tween 20) was made with 1× phosphate buffered saline (without calcium and magnesium, Corning) and 0.05% (v/v) Tween 20 (Sigma-Aldrich).

Particle Synthesis: All particles were fabricated via stop flow lithography as previously described,[4,42] using a prepolymer composition of 30% PEGDA, 30% AAc, 30% poly(ethylene glycol) (PEG), 5% rhodamine acrylate solution, and 5% photoinitiator (Darocur 1173), by volume. All particles were synthesized in 30 µm tall rectangular PDMS (Sylgard 184, Dow Corning) microfluidic channels bonded on PDMS-coated glass slides. Particles were polymerized by UV light (Lumen 200 metal arc lamp, Prior Scientific) through a UV filter set (11000v3-UV, Chroma Technology, 365 nm, 150 ms exposure time, 2200 mW cm^{-2}) in a mask-defined shape (designed using AutoCAD, printed by Fineline Imaging), and the particles were collected in a microcentrifuge tube filled with PBST. Particles were rinsed eight times with PBST by centrifugation and stored in PBST at 4 °C.

Particle Functionalization: All particle functionalization steps were carried out at a particle concentration between 5000 and 10 000 particles mL^{-1} in PBS. EDC and NHS were dissolved separately in PBS and stock solutions were added to the washed particles to achieve final concentrations of 3.3 mg mL^{-1} each. The solution was vortexed for 30 s and placed on a horizontal shaker (650 rpm) at room temperature for 30 min. After activation, particles were rinsed four times in PBST by centrifugation. After washing, NeutrAvidin stock solution was added to the particles to achieve a final protein concentration of 0.83 mg mL^{-1} and the solution was incubated on a horizontal shaker for 2.5 h (650 rpm, room temperature). The particles were rinsed four times in PBST and anti-EpCAM biotin was added to achieve a concentration of 0.083 mg mL^{-1}. The solution was incubated on a horizontal shaker for 30 min (650 rpm, room temperature). Particles were rinsed four times and stored in PBST at 4 °C.

Cell Culture: High-EpCAM-expressing breast cancer (SKBR3) and non-EpCAM-expressing melanoma (SKMEL28) cell lines were obtained from the American Type Culture Collection (ATCC) and cultured according to standard culture protocols. Standard culture media comprised McCoy's 5A (ATCC) or Eagle's Minimum Essential Medium (EMEM; ATCC) supplemented with 10% fetal bovine serum (Life Technologies) and 1% penicillin-streptomycin (Life Technologies), for SKBR3 and SKMEL28 lines, respectively. Cells were grown in 25 cm^2 rectangular canted-neck cell culture flasks with vent-caps (Corning Life Sciences) at 37 °C and 5% carbon dioxide, and were either passaged or used at 85% confluency. For cell–particle experiments, cells were stained using CellTracker Green CMFDA (5-chloromethylfluorescein diacetate; $\lambda_{ex}/\lambda_{em}$ = 492/517 nm, Life Technologies), CellTracker Blue CMAC (7-amino-4-chloromethylcoumarin; $\lambda_{ex}/\lambda_{em}$ = 353/466 nm, Life Technologies), or Hoechst 33342 ($\lambda_{ex}/\lambda_{em}$ = 350/461 nm, Life Technologies) following manufacturer's instructions. Cells were subsequently trypsinized using 0.05% trypsin-EDTA (ethylenediaminetetraacetic acid) (Life Technologies), and then resuspended in media at a concentration of 1 million cells mL^{-1}.

Cell–Particle Experiments: Particles (600 particles mL^{-1}) and cells (400 000 cells mL^{-1} in 50% media, 50% PBST, by volume for all experiments, except Figure 2C,D that uses 100 000 total cells mL^{-1}) were incubated together for 2 h at room temperature, under gentle agitation. Total solution volumes were ≈1 mL. Before imaging, solutions were vortexed gently to remove nonadherent cells from particles.

Imaging and Flow Experiments: Epifluorescence and bright-field images were taken using an inverted microscope (Axio Observer.A1, Zeiss; 10× and 20× objectives) connected to a cooled interline CCD (charge-coupled device) camera (Clara, Andor). Videos of microfluidic flow experiments were taken using high-speed cameras (Phantom v4.2 and Phantom Miro M310, Vision Research) at frame rates ranging from 2000 to 8500 fps and exposure times ranging from 2 to 10 µs.

Supporting Information

Supporting Information is available from the Wiley Online Library or from the author.

DOI: 10.1002/smll.201600163

Acknowledgments

L.C. and H.Z.A. contributed equally to this work. This work was supported in part by the MRSEC Program of the National Science Foundation under award number DMR-1419807, the National Science Foundation CMMI-1120724, and Institute for Collaborative Biotechnologies through grant W911NF-09-0001 from the U.S. Army Research Office. The content of the information does not necessarily reflect the position or the policy of the Government, and no official endorsement should be inferred. Additional support was provided by the US National Institutes of Health (NIH) P41 Resource Center and an NIH National Institute of Biomedical Imaging and Bioengineering Quantum Grant. The authors thank Octavio Hurtado for help with device microfabrication, and Aimal H. Khankhel for help with cell culture. L.C. was supported in part by a postgraduate scholarship from Natural Sciences and Engineering Research Council (NSERC) of Canada.

[1] S. Mitragotri, J. Lahann, *Adv. Mater.* **2012**, *24*, 3717.
[2] J. P. Best, Y. Yan, F. Caruso, *Adv. Healthcare Mater.* **2012**, *1*, 35.
[3] Y. Geng, P. Dalhaimer, S. Cai, R. Tsai, M. Tewari, T. Minko, D. E. Discher, *Nat. Nanotechnol.* **2007**, *2*, 249.
[4] D. Dendukuri, D. C. Pregibon, J. Collins, T. A. Hatton, P. S. Doyle, *Nat. Mater.* **2006**, *5*, 365.
[5] H. C. Shum, A. R. Abate, D. Lee, A. R. Studart, B. Wang, C.-H. Chen, J. Thiele, R. K. Shah, A. Krummel, D. A. Weitz, *Macromol. Rapid Commun.* **2010**, *31*, 108.
[6] J. Rolland, B. Maynor, L. Euliss, A. Exner, G. Denison, J. DeSimone, *J. Am. Chem. Soc.* **2005**, *127*, 10096.
[7] S. Bhaskar, K. M. Pollock, M. Yoshida, J. Lahann, *Small* **2010**, *6*, 404.
[8] J. A. Champion, Y. K. Katare, S. Mitragotri, *Proc. Natl. Acad. Sci. USA* **2007**, *104*, 11901.
[9] T. J. Merkel, S. W. Jones, K. P. Herlihy, F. R. Kersey, A. R. Shields, M. Napier, J. C. Luft, H. Wu, W. C. Zamboni, A. Z. Wang, J. E. Bear, J. M. DeSimone, *Proc. Natl. Acad. Sci. USA* **2011**, *108*, 586.
[10] S. E. A. Gratton, P. A. Ropp, P. D. Pohlhaus, J. C. Luft, V. J. Madden, M. E. Napier, J. M. DeSimone, *Proc. Natl. Acad. Sci. USA* **2008**, *105*, 11613.
[11] V. Uskoković, K. Lee, P. P. Lee, K. E. Fischer, T. A. Desai, *ACS Nano* **2012**, *6*, 7832.
[12] A. C. Anselmo, M. Zhang, S. Kumar, D. R. Vogus, S. Menegatti, M. E. Helgeson, S. Mitragotri, *ACS Nano* **2015**, *9*, 3169.
[13] J. A. Champion, S. Mitragotri, *Proc. Natl. Acad. Sci. USA* **2006**, *103*, 4930.
[14] S. Barua, J. Yoo, P. Kolhar, A. Wakankar, Y. R. Gokarn, S. Mitragotri, *Proc. Natl. Acad. Sci. USA* **2013**, *110*, 3270.
[15] K. K. Zeming, S. Ranjan, Y. Zhang, *Nat. Commun.* **2013**, *4*, 1625.
[16] S. Ranjan, K. K. Zeming, R. Jureen, D. Fisher, Y. Zhang, *Lab Chip* **2014**, *14*, 4250.
[17] Y.-Q. Li, B. K. Chandran, C. T. Lim, X. Chen, *Adv. Sci.* **2015**, *2*, 10.1002/advs.201500118.
[18] A. L. Bole, P. Manesiotis, *Adv. Mater.* **2015**, DOI: 10.1002/adma.201503962.
[19] P. S. Steeg, *Nat. Med.* **2006**, *12*, 895.
[20] K. Pantel, R. H. Brakenhoff, *Nat. Rev. Cancer* **2004**, *4*, 448.
[21] J. den Toonder, *Lab Chip* **2011**, *11*, 375.
[22] Z. T. F. Yu, K. M. Aw Yong, J. Fu, *Small* **2014**, *10*, 1687.
[23] S. L. Stott, C.-H. Hsu, D. I. Tsukrov, M. Yu, D. T. Miyamoto, B. A. Waltman, S. M. Rothenberg, A. M. Shah, M. E. Smas, G. K. Korir, F. P. Floyd, A. J. Gilman, J. B. Lord, D. Winokur, S. Springer, D. Irimia, S. Nagrath, L. V. Sequist, R. J. Lee, K. J. Isselbacher, S. Maheswaran, D. A. Haber, M. Toner, *Proc. Natl. Acad. Sci. USA* **2010**, *107*, 18392.
[24] A. M. Shah, M. Yu, Z. Nakamura, J. Ciciliano, M. Ulman, K. Kotz, S. L. Stott, S. Maheswaran, D. A. Haber, M. Toner, *Anal. Chem.* **2012**, *84*, 3682.
[25] S. Nagrath, L. V Sequist, S. Maheswaran, D. W. Bell, D. Irimia, L. Ulkus, M. R. Smith, E. L. Kwak, S. Digumarthy, A. Muzikansky, P. Ryan, U. J. Balis, R. G. Tompkins, D. A. Haber, M. Toner, *Nature* **2007**, *450*, 1235.
[26] S. Wang, H. Wang, J. Jiao, K. J. Chen, G. E. Owens, K. I. Kamei, J. Sun, D. J. Sherman, C. P. Behrenbruch, H. Wu, H. R. Tseng, *Angew. Chem., Int. Ed.* **2009**, *48*, 8970.
[27] B. D. Plouffe, S. K. Murthy, L. H. Lewis, *Rep. Prog. Phys.* **2015**, *78*, 016601.
[28] H. W. Hou, M. E. Warkiani, B. L. Khoo, Z. R. Li, R. A. Soo, D. S.-W. Tan, W.-T. Lim, J. Han, A. A. S. Bhagat, C. T. Lim, *Sci. Rep.* **2013**, *3*, 1.
[29] J. Chen, J. Li, Y. Sun, *Lab Chip* **2012**, *12*, 1753.
[30] W. Qian, Y. Zhang, W. Chen, *Small* **2015**, *11*, 3850.
[31] E. Ozkumur, A. M. Shah, J. C. Ciciliano, B. L. Emmink, D. T. Miyamoto, E. Brachtel, M. Yu, P. Chen, B. Morgan, J. Trautwein, A. Kimura, S. Sengupta, S. L. Stott, N. M. Karabacak, T. A. Barber, J. R. Walsh, K. Smith, P. S. Spuhler, J. P. Sullivan, R. J. Lee, D. T. Ting, X. Luo, A. T. Shaw, A. Bardia, L. V Sequist, D. N. Louis, S. Maheswaran, R. Kapur, D. A. Haber, M. Toner, *Sci. Transl. Med.* **2013**, *5*, 179ra47.
[32] N. M. Karabacak, P. S. Spuhler, F. Fachin, E. J. Lim, V. Pai, E. Ozkumur, J. M. Martel, N. Kojic, K. Smith, P. Chen, J. Yang, H. Hwang, B. Morgan, J. Trautwein, T. A. Barber, S. L. Stott, S. Maheswaran, R. Kapur, D. A. Haber, M. Toner, *Nat. Protoc.* **2014**, *9*, 694.
[33] M. Yu, S. Stott, M. Toner, S. Maheswaran, D. A. Haber, *J. Cell Biol.* **2011**, *192*, 373.
[34] D. Horak, Z. Svobodova, J. Autebert, B. Coudert, Z. Plichta, K. Kralovec, Z. Bílková, J. L. Viovy, *J. Biomed. Mater. Res., Part A* **2013**, *101 A*, 23.
[35] C. Arya, J. G. Kralj, K. Jiang, M. S. Munson, T. P. Forbes, D. L. DeVoe, S. R. Raghavan, S. P. Forry, *J. Mater. Chem. B* **2013**, *1*, 4313.
[36] K. Hoshino, Y.-Y. Huang, N. Lane, M. Huebschman, J. W. Uhr, E. P. Frenkel, X. Zhang, *Lab Chip* **2011**, *11*, 3449.
[37] R. L. Srinivas, S. C. Chapin, P. S. Doyle, *Anal. Chem.* **2011**, *83*, 9138.
[38] D. C. Pregibon, M. Toner, P. S. Doyle, *Science* **2007**, *315*, 1393.
[39] S. K. Suh, K. Yuet, D. K. Hwang, K. W. Bong, P. S. Doyle, T. A. Hatton, *J. Am. Chem. Soc.* **2012**, *134*, 7337.
[40] H. Z. An, M. E. Helgeson, P. S. Doyle, *Adv. Mater.* **2012**, *24*, 3838.
[41] P. T. H. Went, A. Lugli, S. Meier, M. Bundi, M. Mirlacher, G. Sauter, S. Dirnhofer, *Hum. Pathol.* **2004**, *35*, 122.
[42] D. Dendukuri, S. S. Gu, D. C. Pregibon, T. A. Hatton, P. S. Doyle, *Lab Chip* **2007**, *7*, 818.
[43] R. Haghgooie, M. Toner, P. S. Doyle, *Macromol. Rapid Commun.* **2010**, *31*, 128.
[44] M. Björnmalm, Y. Yan, F. Caruso, *J. Controlled Release* **2014**, *190*, 139.
[45] N. W. Choi, J. Kim, S. C. Chapin, T. Duong, E. Donohue, P. Pandey, W. Broom, W. A. Hill, P. S. Doyle, *Anal. Chem.* **2012**, *84*, 9370.
[46] N. Nakajima, Y. Ikada, *Bioconjugate Chem.* **1995**, *6*, 123.
[47] E. Friederich, D. Louvard, in *Encyclopedic Reference of Genomics and Proteomics in Molecular Medicine* (Eds: D. Ganten, K. Ruckpaul), Springer,Berlin **2006**, p. 1116.
[48] W. Wu, W. Wang, J. Li, *Prog. Polym. Sci.* **2015**, *46*, 55.
[49] P. Joshi, B. Jacobs, A. Derakhshan, L. R. Moore, P. Elson, P. L. Triozzi, E. Borden, M. Zborowski, *Oncotarget* **2014**, *5*, 2450.
[50] A. Martowicz, G. Spizzo, G. Gastl, G. Untergasser, *BMC Cancer* **2012**, *12*, 501.

[51] H. Z. An, H. B. Eral, L. Chen, M. B. Chen, P. S. Doyle, *Soft Matter* **2014**, *10*, 7595.
[52] P. Fischer, M. Tibbitt, A. Kloxin, K. S. Anseth, J. Oakey, *Biomed. Sci. Instrum.* **2014**, *50*, 62.
[53] D. S. Shin, J. You, A. Rahimian, T. Vu, C. Siltanen, A. Ehsanipour, G. Stybayeva, J. Sutcliffe, A. Revzin, *Angew. Chem., Int. Ed.* **2014**, *53*, 8221.
[54] A. Hatch, G. Hansmann, S. K. Murthy, *Langmuir* **2011**, *27*, 4257.
[55] A. Khademhosseini, J. Yeh, S. Jon, G. Eng, K. Y. Suh, J. A. Burdick, R. Langer, *Lab Chip* **2004**, *4*, 425.
[56] G. C. Le Goff, J. Lee, A. Gupta, W. A. Hill, P. S. Doyle, *Adv. Sci.* **2015**, *2*, DOI: 10.1002/advs.201500149.
[57] J. P. Gleghorn, E. D. Pratt, D. Denning, H. Liu, N. H. Bander, S. T. Tagawa, D. M. Nanus, P. A. Giannakakou, B. J. Kirby, *Lab Chip* **2010**, *10*, 27.
[58] A. M. Malek, S. L. Alper, S. Izumo, *J. Am. Med. Assoc.* **1999**, *282*, 2035.
[59] K. W. Bong, J. J. Kim, H. Cho, E. Lim, P. S. Doyle, D. Irimia, *Langmuir* **2015**, *31*, 13165.
[60] J. Lee, P. W. Bisso, R. L. Srinivas, J. J. Kim, A. J. Swiston, P. S. Doyle, *Nat. Mater.* **2014**, *13*, 524.
[61] F. Zheng, Y. Cheng, J. Wang, J. Lu, B. Zhang, Y. Zhao, Z. Gu, *Adv. Mater.* **2014**, *26*, 7333.

Received: January 18, 2016
Published online: